Photochemical & Photobiological Sciences

PAPER

Cite this: *Photochem. Photobiol. Sci.*, 2017, **16**, 1449

Photophysical properties of hexyl diethylaminohydroxybenzoylbenzoate (Uvinul A Plus), a UV-A absorber†

Yuta Shamoto, [a] Mikio Yagi, *[a] Nozomi Oguchi-Fujiyama, [b] Kazuyuki Miyazawa [b] and Azusa Kikuchi *[a]

Received 9th May 2017,
Accepted 22nd July 2017

DOI: 10.1039/c7pp00164a

rsc.li/pps

Hexyl diethylaminohydroxybenzoylbenzoate (DHHB, Uvinul A Plus) is a photostable UV-A absorber. The photophysical properties of DHHB have been studied by obtaining the transient absorption, total emission, phosphorescence and electron paramagnetic resonance spectra. DHHB exhibits an intense phosphorescence in a hydrogen-bonding solvent (*e.g.*, ethanol) at 77 K, whereas it is weakly phosphorescent in a non-hydrogen-bonding solvent (*e.g.*, 3-methylpentane). The triplet–triplet absorption and EPR spectra for the lowest excited triplet state of DHHB were observed in ethanol, while they were not observed in 3-methylpentane. These results are explained by the proposal that in the benzophenone derivatives possessing an intramolecular hydrogen bond, intramolecular proton transfer is an efficient mechanism of the very fast radiationless decay from the excited singlet state. The energy level of the lowest excited triplet state of DHHB is higher than those of the most widely used UV-B absorbers, octyl methoxycinnamate (OMC) and octocrylene (OCR). DHHB may act as a triplet energy donor for OMC and OCR in the mixtures of UV-A and UV-B absorbers. The bimolecular rate constant for the quenching of singlet oxygen by DHHB was determined by measuring the near-IR phosphorescence of singlet oxygen. The photophysical properties of diethylaminohydroxybenzoylbenzoic acid (DHBA) have been studied for comparison. It is a closely related building block to assist in interpreting the observed data.

Introduction

UV solar radiation is divided into three types. The most energetic UV radiation is UV-C (100–280 nm). UV-C is filtered out in the upper layers of the earth's atmosphere by the ozone layer. The UV radiation that penetrates the ozone layer and reaches the earth's surface is UV-B (280–320 nm) and UV-A (320–400 nm). UV-B radiation is sufficiently energetic and responsible for sunburn, while UV-A radiation is energetically weaker. Over the past several decades, UV-A radiation was considered to be relatively harmless. However, UV-A radiation penetrates deep into the dermis layer of the skin and increases the incidence of skin cancer.[1–5] UV-A radiation is the most abundant UV solar radiation (above 90%) that reaches the surface of the earth.[6] As a consequence of the deleterious effect of UV-A radiation, UV-A protection has become a target for sunscreen efficacy.

In response to the increasing awareness of the deleterious effect of UV-A radiation, several UV-A absorbers became available for the formulation of cosmetic sunscreens. Practically, 4-*tert*-butyl-4′-methoxydibenzoylmethane (BMDBM, trade names: Parsol 1789 and Eusolex 9020) is one of the most widely used UV-A absorbers in the world. The photochemical and photophysical properties of BMDBM have been extensively studied.[7–11] BMDBM has a high molar extinction coefficient in the UV-A region (30 500 mol^{-1} dm^3 cm^{-1} at 357 nm), but it suffers from photoinstability.[12,13] A number of studies have been devoted to photostabilize BMDBM.[13–22]

Hexyl diethylaminohydroxybenzoylbenzoate (DHHB, trade name Uvinul A Plus, Scheme 1) is a successor to BMDBM.[15,23–27] The photostability of DHHB is superior to that of BMDBM.[28] DHHB is approved for use (up to 10%) in Australia/New Zealand, Brazil, EU, Japan and South Africa.[29–31] However, to the best of our knowledge, very little information on the photophysical properties of DHHB has been reported in the scientific literature.[32,33]

[a]*Department of Chemistry, Graduate School of Engineering, Yokohama National University, Tokiwadai, Hodogaya-ku, Yokohama 240-8501, Japan. E-mail: yagi-mikio-sc@ynu.ac.jp, kikuchi-azusa-rh@ynu.ac.jp*

[b]*Shiseido Research Center, Hayabuchi, Tsuzuki-ku, Yokohama 224-8558, Japan*

†Electronic supplementary information (ESI) available: The UV absorption, total emission and phosphorescence spectra of DHBA in EtOH. The phosphorescence spectrum and variation of the phosphorescence intensity of DHHB in 3-MP at 77 K. The computer-simulated time-resolved EPR spectra of DHHB. The transient absorption spectrum of DHHB in Ar-saturated ethylene glycol at 25 °C. See DOI: 10.1039/c7pp00164a

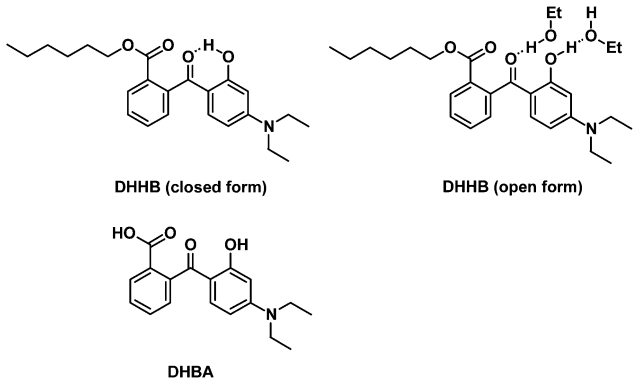

Scheme 1 Molecular structures of DHHB (Uvinul A plus) and DHBA.

In the present study, we have studied the photophysical properties of DHHB through the analysis of the transient absorption, total emission, phosphorescence and electron paramagnetic resonance (EPR) spectra. The rate constant for the quenching of singlet oxygen by DHHB was determined. The photophysical properties of diethylaminohydroxybenzoylbenzoic acid (DHBA, Scheme 1) have been studied for comparison. It is a closely related building block to assist in interpreting the observed data.

Experimental

Chemicals

DHHB (BASF Japan, 99.7%), DHBA (TCI EP Grade, >98.0%), ethanol (EtOH, Wako Super Special Grade, 99.5%) and 3-methylpentane (3-MP, TCI GR Grade, >99.0%) were used as received.

Optical measurements

The details of the UV absorption, transient absorption, total emission, phosphorescence and time-resolved near-IR phosphorescence measurements have been described previously.[34–37] For the transient absorption measurements, a Continuum Surelite Nd:YAG laser (355 nm) was used as an exciting light source with a repetition rate of 10 Hz. For the quenching measurements of singlet oxygen, samples were excited with the Continuum Surelite Nd:YAG laser (532 nm, repetition rate 10 Hz).

EPR measurements

The experimental setup for the EPR measurements is the same as that reported previously.[34,35] For the time-resolved EPR measurements, samples were excited with the Continuum Surelite Nd:YAG laser (355 nm, repetition rate 10 Hz).

Results and discussion

UV absorption spectra

The UV absorption spectra of DHHB and DHBA were obtained in EtOH at 25 °C and 77 K. DHHB absorbs UV-A radiation with a peak at 354 nm, as shown in Fig. 1a. The molar absorption coefficient of DHHB in EtOH at 25 °C was obtained to be 39 000 mol^{-1} dm^3 cm^{-1} at 354 nm. The UV absorption spectrum of DHBA is similar to that of DHHB, but slightly blue-shifted with regard to that of DHHB, as shown in Fig. S1.† The molar absorption coefficient of DHBA in EtOH at 25 °C was obtained to be 36 000 mol^{-1} dm^3 cm^{-1} at 350 nm.

At 77 K, the UV absorption spectrum of DHHB slightly red-shifted with a peak at 360 nm. After UV irradiation for 60 min (at 77 K, 365 nm Hg lamp), the spectrum blue-shifted remarkably with a peak at 340 nm, as shown in Fig. 1b. This photo-

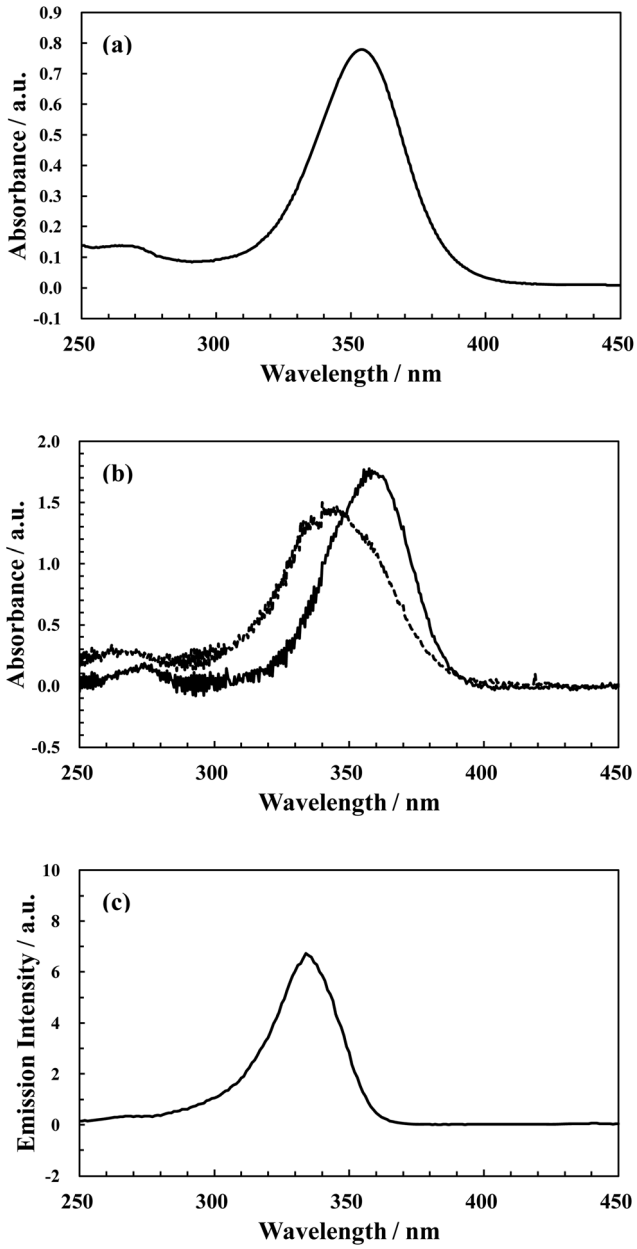

Fig. 1 UV absorption spectra of DHHB in EtOH (a) at 25 °C before irradiation and (b) at 77 K before (A: solid line) and after (B: broken line) UV irradiation at 365 nm for 60 min. (c) Phosphorescence–excitation (λ_{obs} = 440 nm) spectrum of DHHB-2 in EtOH at 77 K.

induced species is hereafter denoted as DHHB-PIS. The properties of DHHB-PIS are discussed in a later section.

Emission spectra

The total emission and phosphorescence spectra of DHHB were obtained through the excitation at 365 nm in EtOH at 77 K. As is clearly seen in Fig. 2, the total emission spectrum consists of a fluorescence spectrum and a phosphorescence spectrum. We used a phosphoroscope and a pair of electromechanical shutters to separate the phosphorescence spectrum from the total emission spectrum. The emission spectrum of DHHB in EtOH is dependent on the excitation wavelength. The blue-shifted total emission and phosphorescence spectra were observed through the excitation at 334 nm in EtOH at 77 K, as shown in Fig. 3. There are at least two emissive species in EtOH at 77 K. The species which has the lower energy levels of the S_1 and T_1 states is denoted hereafter as DHHB-1 and the species which has the higher energy levels is hereafter denoted as DHHB-2. The conformations of DHHB-1 and DHHB-2 seem to be unclear at this stage. The emission and phosphorescence spectra of DHBA are also dependent on the excitation wavelength, as shown in Fig. S2 and S3.†

To clarify the properties of DHHB-1 and DHHB-2, the irradiation time dependence of the phosphorescence intensity

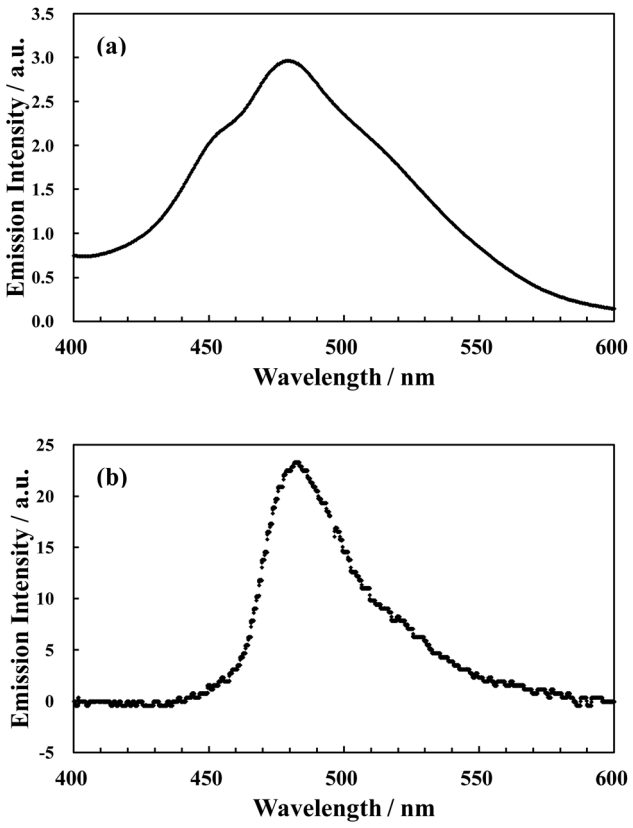

Fig. 2 (a) Total emission and (b) time-resolved phosphorescence spectra of DHHB in EtOH at 77 K through the excitation at 365 nm. The sampling times were set at 0.80–0.96 s after shutting off the exciting light for the time-resolved phosphorescence measurements.

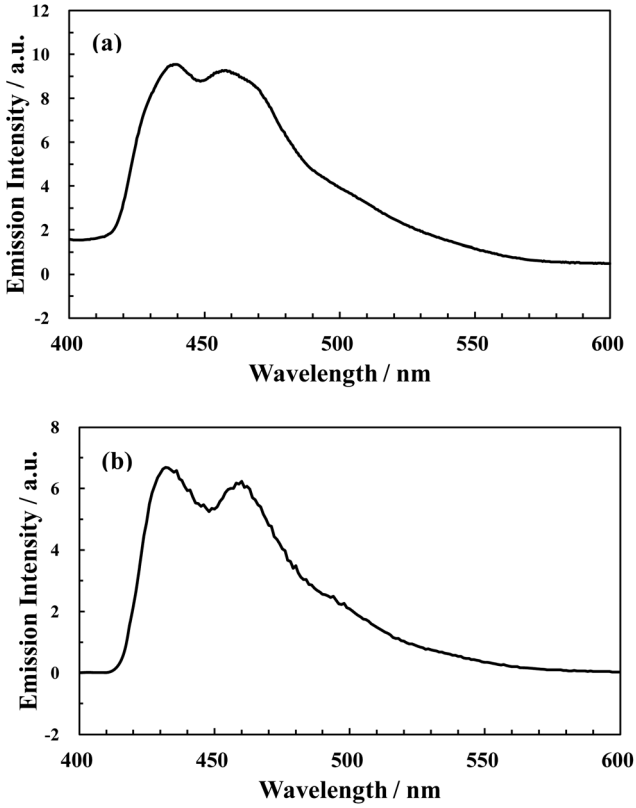

Fig. 3 (a) Total emission and (b) phosphorescence spectra of DHHB in EtOH at 77 K through the excitation at 334 nm.

was observed. It is seen in Fig. 4 that the phosphorescence intensity of DHHB-1 increases quickly and decreases gradually. On the other hand, no phosphorescence of DHHB-2 is detected at the very beginning of irradiation. This means that DHHB-2 is not present before irradiation. The phosphorescent DHHB-2 is produced by irradiation. In Fig. 1c the phosphorescence–excitation spectrum of DHHB-2 in EtOH at 77 K is shown. The observed spectrum is similar to the absorption spectrum of DHHB-PIS. Therefore DHHB-1 and DHHB-2 are safely assigned to DHHB and DHHB-PIS, respectively. Similar irradiation time dependence of the phosphorescence intensity was observed for DHBA in EtOH at 77 K, as shown in Fig. S4.†

To obtain more information on the possible structure of DHHB-PIS, phosphorescence measurements were carried out after a dark period of three hours in EtOH at 77 K. The phosphorescence intensity of DHHB-PIS increases quickly as observed at the end of the preceding irradiation period. The irradiation time dependence of the phosphorescence intensity is not reversible at 77 K. DHHB-PIS is most likely assigned to a photoproduct.

After extensive irradiation at 77 K, the sample solution was heated to room temperature during a dark period of three hours and then cooled down again to 77 K. No phosphorescence of DHHB-PIS was detected at the very beginning of irradiation, as shown in Fig. S5.† The irradiation time dependence of the phosphorescence intensity is reversible after a

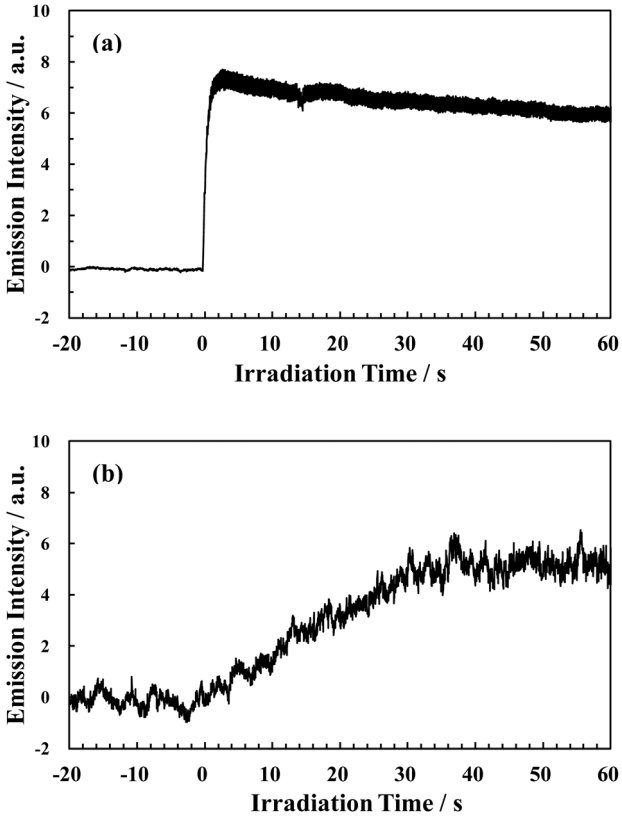

Fig. 4 Variation of the phosphorescence intensity of DHHB with irradiation time in EtOH at 77 K. The samples were excited at 365 nm. Phosphorescence was monitored at (a) 480 nm and (b) 440 nm.

dark period at room temperature. DHHB-PIS is stable at 77 K, but it comes back to original DHHB at room temperature. The observed reversibility of the formation of DHHB-PIS at room temperature is consistent with the reported photostability of DHHB. Binks *et al.* reported that extensive irradiation of DHHB solutions at room temperature caused no changes in the UV absorption spectra.[28]

The phosphorescence lifetime of DHHB is longer than that of DHHB-PIS. Therefore, the "pure" phosphorescence spectrum of DHHB can be separated from the "mixed" phosphorescence spectrum of DHHB and DHHB-PIS by setting the sampling time sufficiently long after shutting off the exciting light. The observed spectrum is shown in Fig. 2b. The energy level of the lowest excited triplet (T_1) state of DHHB was estimated to be 20 700 cm^{-1} from the first peak of phosphorescence. The lifetime of the T_1 state of DHHB was obtained to be 0.7 s from the decay of phosphorescence. The T_1 energy of DHHB is higher than those of the most widely UV-B absorbers, octyl methoxycinnamate (OMC, trade names: Parasol MCX, Neo Heliopan AV and Uvinul MC80, E_{T_1} = 19 500 cm^{-1}) and octocrylene (OCR, trade names: Escalol 597 and Neo Heliopan 303, E_{T_1} < 20 400 cm^{-1}).[10] DHHB may act as a triplet energy donor for OMC and OCR in the mixtures of UV-A and UV-B absorbers. OMC alone undergoes *trans* to *cis* photoisomerization.[38] The molar absorption coefficient of *cis*-OMC is lower than that of *trans*-OMC.[38] Therefore, DHHB may decrease the efficiency of OMC as a UV-B absorber in the mixture of DHHB and OMC.

The energy level of the T_1 state of DHHB-PIS was estimated to be 23 100 cm^{-1} from the first peak of phosphorescence observed through the excitation at 334 nm. The T_1 lifetime of DHHB-PIS was estimated from the phosphorescence decay at 440 nm to be 0.1 s, although the phosphorescence decays slightly deviate from the single-exponential decays.

The phosphorescence spectra of DHHB were observed in 3-MP at 77 K, as shown in Fig. 5. The phosphorescence in 3-MP is much weaker than that in EtOH. DHHB is a 2-hydroxybenzophenone derivative with the proximity of the carbonyl and hydroxyl groups permitting intramolecular and intermolecular hydrogen bonds as shown in the chemical structure (Scheme 1). The most plausible explanation for the weak phosphorescence in 3-MP is as follows. In 3-MP, DHHB is in an intramolecularly hydrogen-bonded form (closed form, Scheme 1) and intramolecular excited-state proton transfer (ESPT) takes place after photoexcitation. Intramolecular ESPT is followed by rapid internal conversion, resulting in excellent photostability of DHHB.[39–43] On the other hand, in EtOH, DHHB is an intermolecularly hydrogen-bonded form (open form, Scheme 1) and DHHB undergoes intersystem crossing to the T_1 state, resulting in strong phosphorescence.

DHHB is a derivative of 2-hydroxybenzophenone. Lamola and Sharp reported that 2-hydroxybenzophenone, 2,2′-dihydroxybenzophenone, 2,4-dihydroxybenzophenone and 2-hydroxy-4-methoxybenzophenone are strongly phosphorescent in 1 : 1 ether–ethanol by volume, but these are very weakly phosphorescent or non-phosphorescent in 3-MP at 77 K.[44] Their explanation for the observed solvent effect on the phosphorescence intensity is also based on intramolecular and intermolecular hydrogen bonds.

Recently, Karsili *et al.* reported the *ab initio* study of the potential ultrafast internal conversion route in 2-hydroxy-4-methoxybenzophenone.[45] They reported that internal conversion is deduced to occur on ultrafast time scales, *via* a barrierless electron-driven hydrogen atom transfer pathway from the

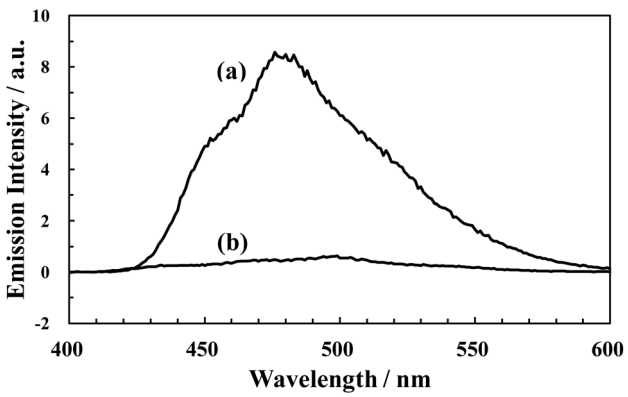

Fig. 5 Phosphorescence spectra of DHHB (a) in EtOH and (b) in 3-MP at 77 K through the excitation at 365 nm.

lowest excited singlet state to a conical intersection with the ground state potential energy surface.

The phosphorescence of DHHB-PIS was also observed in 3-MP at 77 K through the excitation at 334 nm, as shown in Fig. S5.† The variation of the phosphorescence intensity of DHHB at 440 nm was measured. It is seen in Fig. S6† that no phosphorescence is detected at the very beginning of irradiation and the phosphorescent DHHB-PIS is produced by irradiation. The phosphorescence of DHHB-PIS through the excitation at 334 nm in 3-MP is comparable in intensity to that in EtOH. This fact suggests that DHHB-PIS is not an intramolecularly hydrogen-bonded form.

EPR spectra

The g-factor of the T_1 state is almost isotropic for most organic molecules in which the spin–orbit interaction is weak. We can safely assume that the g value is isotropic and equals that of a free electron for DHHB. The electron spin–spin interaction of the T_1 state in an applied magnetic field $\boldsymbol{B}$ is described by the spin Hamiltonian

$$\begin{aligned} H_S &= g\mu_B \boldsymbol{B}\cdot\boldsymbol{S} + \boldsymbol{S}\cdot\boldsymbol{D}\cdot\boldsymbol{S} \\ &= g\mu_B \boldsymbol{B}\cdot\boldsymbol{S} - XS_x^2 - YS_y^2 - ZS_z^2 \\ &= g\mu_B \boldsymbol{B}\cdot\boldsymbol{S} + D\left[S_z^2 - (1/3)\boldsymbol{S}^2\right] + E(S_x^2 - S_y^2). \end{aligned} \quad (1)$$

In this expression, X, Y and Z are equal to the energies of the three triplet sublevels in zero field. The zero-field splitting (ZFS) parameters D, E and D^* are related to be $D = -3Z/2$, $E = (Y - X)/2$ and $D^* = (D^2 + 3E^2)^{1/2}$.

Fig. 6 shows the steady-state EPR spectra of the T_1 state of DHHB in EtOH at 77 K. The $\Delta M_S = \pm 1$ transition signals are too weak to be observed in the steady-state EPR measurements. Only a B_{min} signal was observed for the T_1 state of DHHB. The resonance field of the B_{min} signal gives the value of D^* through the following equation:[46]

$$D^* = \{(3/4)(h\nu)^2 - 3(g\mu_B B_{min})^2\}^{1/2} \quad (2)$$

where h and ν have their usual meaning.

The steady-state EPR spectra were obtained in EtOH at 77 K using an Asahi Spectra REX-250 250 W Hg lamp as an excitation light source. The steady-state EPR spectrum depends on the excitation wavelength, as shown in Fig. 6. For the time profile measurements of the steady-state EPR signals, a Canrad-Hanovia Xe–Hg lamp of 1 kW was used at 500 W equipped with Asahi Technoglass UV-D33S (transmits the wavelength 250–400 nm) and UV-37 (cuts off the wavelength shorter than 340 nm) glass filters. The T_1 lifetime obtained from the decay of the steady-state B_{min} signal at 149 mT through the excitation at wavelengths 340–400 nm is 0.7 s. The observed T_1 lifetime is in good agreement with that obtained from the phosphorescence decay through the excitation at 365 nm. We can safely assign the steady-state B_{min} signal at 149 mT to DHHB. The value of D^* of DHHB was estimated to be 0.1012 cm^{-1}.

On the other hand, the T_1 lifetime obtained from the decay of the steady-state B_{min} signal at 160 mT through the excitation at wavelengths 250–400 nm is ~0.1 s. As mentioned in the previous section, both DHHB and DHHB-PIS are excited at wavelength 334 nm and DHHB-PIS has a shorter T_1 lifetime of 0.1 s in EtOH at 77 K. We can safely assume that the linewidth of the steady-state B_{min} signal of DHHB-PIS is wider than that of DHHB and the D^* value of DHHB-PIS is smaller than that of DHHB. The intensity of the steady-state EPR signal of DHHB-PIS is weaker than that of DHHB while the phosphorescence intensity of DHHB-PIS is stronger than that of DHHB, as shown in Fig. 3b and 6b. The weak EPR signal of DHHB-PIS can be explained by the fact that the T_1 lifetime of DHHB-PIS is much shorter than that of DHHB.

Only one set of time-resolved EPR signals was observed through the excitation at 355 nm in EtOH at 77 K, as shown in Fig. 7. The polarities of the $\Delta M_S = \pm 1$ transition signals at the stationary fields are EA/EA from the low-field to the high-field. Here A and E denote an absorption and an emission of the microwaves, respectively.

The $|D|$, $|E|$ and D^* values obtained from the stationary fields of the $\Delta M_S = \pm 1$ transition signals are 0.0709 cm^{-1}, 0.0317 cm^{-1} and 0.0896 cm^{-1}, respectively. The D^* value obtained from the time-resolved EPR measurements is much smaller than that of DHHB obtained from the steady-state EPR

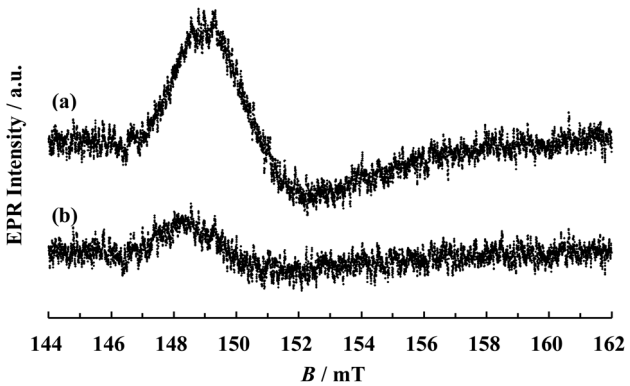

Fig. 6 Steady-state EPR spectra for the T_1 state of DHHB in EtOH at 77 K through the excitation at (a) 365 nm and (b) 334 nm.

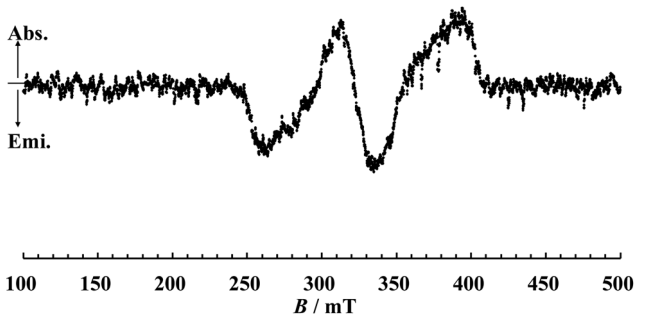

Fig. 7 Time-resolved EPR spectrum for the T_1 state of DHHB-PIS in EtOH at 77 K. The sampling times were set at 0.3–1.3 μs after the 355 nm laser pulse.

measurements. Therefore, we assume that the time-resolved EPR spectrum is ascribed to the T_1 state of DHHB-PIS. In general, the intensity of the time-resolved EPR signal does not depend on the T_1 lifetime. It depends on the anisotropy in the $S_1 \rightarrow T_1$ intersystem crossing. This may be the reason why the EPR spectrum of DHHB-PIS was observed in the time-resolved measurements. One possible explanation for the absence of the EPR signals of DHHB in the time-resolved measurements is that the $S_1 \rightarrow T_1$ intersystem crossing of DHHB is nearly isotropic.

The intersystem crossing rate constants to the three T_1 sublevels are different. The different populations of sublevels are expressed by relative populating rates of the three T_1 sublevels, P_x, P_y and P_z. The anisotropy in the $S_1 \rightarrow T_1$ intersystem crossing of DHHB-PIS was estimated by the computer simulation.[34,35] The results are shown in Fig. S7.† The relative populating rates were estimated to be $(P_x - P_z):(P_y - P_z) = 0.25:0.75$. The $S_1 \rightarrow T_1$ intersystem crossing of DHHB-PIS is highly anisotropic. We can confirm the facts that the EPR signal of DHHB-PIS with a shorter T_1 lifetime is weak in the steady-state measurements but strong in the time-resolved measurements.

Transient absorption spectra

Triplet-state formation at room temperature was examined by nanosecond transient absorption spectroscopy. Fig. 8 shows the transient absorption spectrum of DHHB in Ar-saturated EtOH obtained 0.3–1.2 μs after the 355 nm laser pulse. Laser excitation gives a broad transient absorption spectrum with a peak at ~390 nm and a bleaching with a peak at ~350 nm. The observed bleaching is due to the depletion of the ground state molecules. In contrast, the transient absorption spectrum was not observed in 3-MP at room temperature. This is consistent with the fact that the EPR spectrum of the T_1 state of DHHB was not observed in 3-MP at 77 K.

As is seen in Fig. 8, the vibrational structure is obscure in EtOH. The transient absorption spectrum of DHHB was obtained in a more viscous solvent. Fig. S8† shows the transient absorption spectrum of DHHB in Ar-saturated ethylene glycol. Although the signal-to-noise ratio of the spectrum observed in ethylene glycol is higher than that observed in EtOH, the vibrational structure is still obscure.

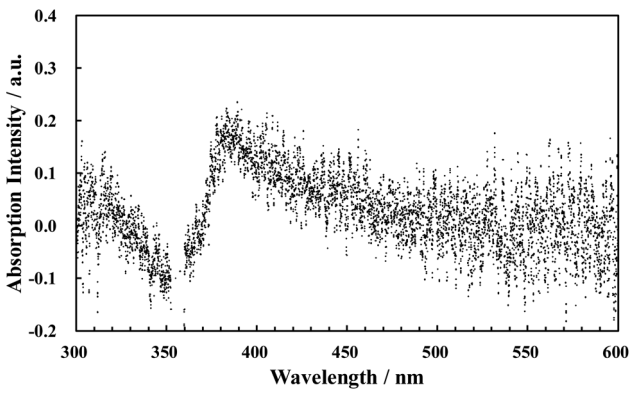

Fig. 8 Transient absorption spectrum of DHHB in Ar-saturated EtOH at 25 °C. The sampling times were set at 0.3–1.2 μs after the 355 nm laser pulse.

Singlet oxygen quenching

In some organic compounds, quenching of the triplet state by ground-state oxygen, $^3O_2(^3\Sigma_g)$, leads to the sensitized formation of singlet oxygen, $^1O_2(^1\Delta_g)$.[47,48] However, the near-IR phosphorescence spectrum of $^1O_2(^1\Delta_g)$ generated by photosensitization with DHHB was not observed in oxygen-saturated EtOH at room temperature.

In order to study the antioxidation effects of DHHB, the rate constant for the quenching of $^1O_2(^1\Delta_g)$ by DHHB was estimated using the following Stern–Volmer equation.[47,49]

$$\tau_0/\tau = 1 + \tau_0\, k_Q\, [Q] \quad (3)$$

In eqn (3), τ_0 and τ are the lifetimes of $^1O_2(^1\Delta_g)$ in the absence and presence of a quencher, respectively; k_Q is the bimolecular rate constant for quenching of $^1O_2(^1\Delta_g)$ by the quencher and [Q] is the concentration of quencher Q.

Singlet oxygen was generated by 532 nm laser irradiation of acetonitrile solutions containing rose bengal and DHHB at room temperature. The lifetimes of $^1O_2(^1\Delta_g)$ generated were measured as a function of the DHHB concentration, as shown in Fig. 9a. The value of τ_0 was obtained to be 73 μs. The bimolecular rate constant for quenching of $^1O_2(^1\Delta_g)$, k_Q, was determined to be 3.5×10^5 mol^{-1} dm^3 s^{-1} using the Stern–Volmer analysis of eqn (3), as shown in Fig. 9b. Lhiaubet-Vallet *et al.* reported that the k_Q value was determined to be *ca.* 10^6 mol^{-1} dm^3 s^{-1} in acetonitrile by using an excimer laser (308 nm) for excitation.[32] The k_Q value obtained in this study is smaller than that reported by Lhiaubet-Vallet *et al.* The rate constant for diffusion in acetonitrile at 25 °C is 1.9×10^{10} mol^{-1} dm^3 s^{-1}.[50] The observed value of k_Q shows that the quenching of singlet oxygen by DHHB is relatively slow. However, the maximum concentration of DHHB authorized in many countries is 10% (0.20 mol dm^{-3} in acetonitrile).[29–31] Using eqn (3), the minimum value of τ/τ_0 is calculated to be 1/6. It should be noted that the lifetime of singlet oxygen is shortened to a sixth by adding 10% DHHB in acetonitrile.

In general, the quenching mechanisms of singlet oxygen are divided into two types: physical quenching and chemical quenching.[47] In the case of DHHB, chemical quenching can be ignored because of the observed photostability of DHHB under our experimental conditions. There are three types of interactions which contribute to physical quenching of singlet oxygen. The rate constants of these processes follow the order (from high to low): (1) electronic energy transfer, (2) charge transfer interactions and (3) electronic-vibrational energy conversion.[47] One of the most effective quenchers of singlet oxygen is β-carotene. The k_Q values of β-carotene have been reported by several groups. Values $0.6 \times 10^{10} \leq k_Q \leq 1.4 \times 10^{10}$ mol^{-1} dm^3 s^{-1} have been observed in solvents of different polarities.[51] The energy level of singlet oxygen, $^1O_2(^1\Delta_g)$, is

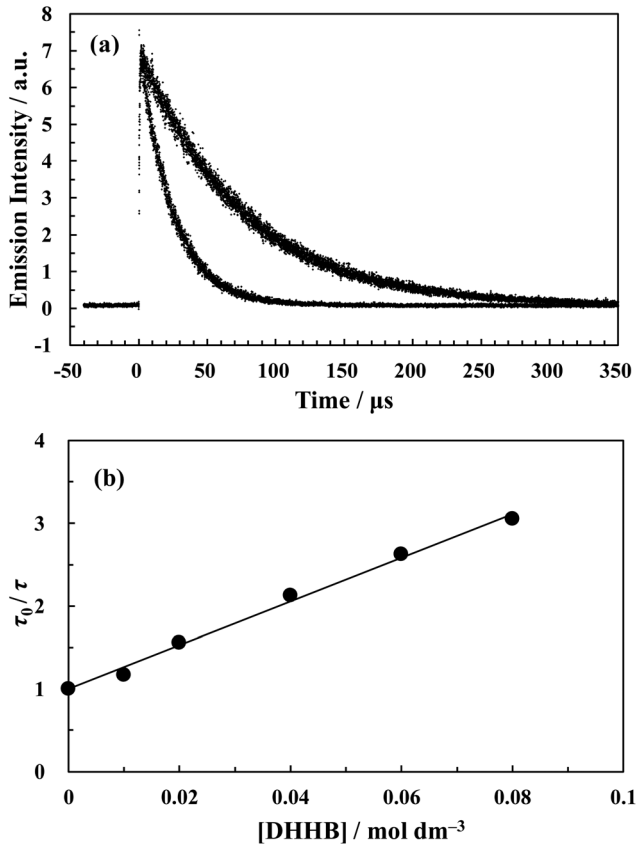

Fig. 9 (a) Time profiles of the phosphorescence intensity of singlet oxygen obtained following 532 nm laser excitation of rose bengal in air-saturated acetonitrile at 25 °C. The faster decay curve was observed in the presence of DHHB (0.08 mol dm^{-3}). The phosphorescence intensity was monitored at 1274 nm. (b) Stern–Volmer plot according to eqn (3) for the quenching of singlet oxygen by DHHB.

7850 cm^{-1}. The energy level of the T_1 state of β-carotene, ~7000 cm^{-1}, is lower than the energy level of singlet oxygen.[47] The electronic energy transfer from singlet oxygen to β-carotene can occur efficiently. On the other hand, the energy level of the T_1 state of DHHB, 20 700 cm^{-1}, is much higher than the energy level of singlet oxygen. The electronic energy transfer from singlet oxygen to DHHB is thermodynamically unfavourable. This is the reason why the quenching of singlet oxygen by DHHB is relatively slow.

Conclusions

The observed T_1 energy of DHHB is higher than those of OMC and OCR. DHHB may act as a triplet energy donor for OMC and OCR in the mixtures of UV-A and UV-B absorbers. Transient absorption and EPR measurements show that the $S_1 \rightarrow T_1$ intersystem crossing is not negligible for DHHB in a hydrogen-bonding solvent. In contrast, intramolecular proton transfer leads to the very fast radiationless decay from the S_1 state in a non-hydrogen-bonding solvent. This rapid dissipation of the absorbed UV-A energy results in high photostability. This is one of the reasons why DHHB is used as a relatively photostable UV-A absorber in sunscreens. The near-IR phosphorescence of singlet oxygen generated by excitation of DHHB was not observed in oxygen-saturated EtOH. DHHB has a relatively slow bimolecular rate constant for quenching of singlet oxygen.

Acknowledgements

This work was supported in part by JSPS KAKENHI Grant Numbers 23241034 and 24655060. This work was also supported in part by the Takahashi Industrial and Economic Research Foundation.

Notes and references

1 N. A. Shaath, Sunscreen Evolution, in *Sunscreens: Regulations and Commercial Development*, ed. N. A. Shaath, Taylor & Francis, Boca Raton, 2005, pp. 3–17.
2 N. R. Attard and P. Karran, UVA photosensitization of thiopurines and skin cancer in organ transplant recipients, *Photochem. Photobiol. Sci.*, 2012, **11**, 62–68.
3 A. Fourtanier, D. Moyal and S. Seite, UVA filters in sunprotection products: regulatory and biological aspects, *Photochem. Photobiol. Sci.*, 2012, **11**, 81–89.
4 G. P. Pfeifer and A. Besaratinia, UV wavelength-dependent DNA damage and human non-melanoma and melanoma skin cancer, *Photochem. Photobiol. Sci.*, 2012, **11**, 90–97.
5 B. Epe, DNA damage spectra induced by photosensitization, *Photochem. Photobiol. Sci.*, 2012, **11**, 98–106.
6 E. Sage, P.-M. Girard and S. Francesconi, Unravelling UVA-induced mutagenesis, *Photochem. Photobiol. Sci.*, 2012, **11**, 74–80.
7 M. Yamaji and M. Kida, Photothermal tautomerization of a UV sunscreen (4-*tert*-butyl-4′-methoxydibenzoylmethane) in acetonitrile studied by steady-state and laser flash photolysis, *J. Phys. Chem. A*, 2013, **117**, 1946–1951.
8 J. Kockler, M. Oelgemöller, S. Robertson and B. D. Glass, Influence of titanium dioxide particle size on the photostability of the chemical UV-filters butyl methoxy dibenzoylmethane and octocrylene in a microemulsion, *Cosmetics*, 2014, **1**, 128–139.
9 L. Pinto da Silva, P. J. O. Ferreira, D. J. R. Duarte, M. S. Miranda and J. C. G. Esteves da Silva, Structural, energetic, and UV–Vis spectral analysis of UVA filter 4-*tert*-butyl-4′-methoxydibenzoylmethane, *J. Phys. Chem. A*, 2014, **118**, 1511–1518.
10 A. Kikuchi, Y. Nakabai, N. Oguchi-Fujiyama, K. Miyazawa and M. Yagi, Energy-donor phosphorescence quenching study of triplet–triplet energy transfer between UV absorbers, *J. Lumin.*, 2015, **166**, 203–208.
11 M. H. Chisholm, C. B. Durr, T. L. Gustafson, W. T. Kender, T. F. Spilker and P. J. Young, Electronic and spectroscopic properties of avobenzone derivatives attached to Mo_2 quadruple

bonds: Suppression of the photochemical enol-to-keto transformation, *J. Am. Chem. Soc.*, 2015, **137**, 5155–5162.
12 N. A. Shaath, The chemistry of ultraviolet filters, in *Sunscreens, Regulations and Commercial Development*, ed. N. A. Shaath, Taylor & Francis, Boca Raton, 2005, pp. 217–238.
13 C. A. Bonda, The photostability of organic sunscreen actives: A review, in *Sunscreens, Regulations and Commercial Development*, ed. N. A. Shaath, Taylor & Francis, Boca Raton, 2005, pp. 321–349.
14 E. Damiani, L. Rosati, R. Castagna, P. Carloni and L. Greci, Changes in ultraviolet absorbance and hence in protective efficacy against lipid peroxidation of organic sunscreens after UVA irradiation, *J. Photochem. Photobiol., B*, 2006, **82**, 204–213.
15 E. Damiani, W. Baschong and L. Greci, UV-Filter combinations under UV-A exposure: Concomitant quantification of over-all spectral stability and molecular integrity, *J. Photochem. Photobiol., B*, 2007, **87**, 95–104.
16 B. Herzog, M. Wehrle and K. Quass, Photostability of UV absorber systems in sunscreens, *Photochem. Photobiol.*, 2009, **85**, 869–878.
17 C. Mendrok-Edinger, K. Smith, A. Janssen and J. Vollhardt, The quest for avobenzone stabilizers and sunscreen photostability, *Cosmet. Toiletries*, 2009, **124**, 47–54.
18 S. Scalia and M. Mezzena, Photostabilization effect of quercetin on the UV filter combination, butyl methoxydibenzoylmethane–octyl methoxycinnamate, *Photochem. Photobiol.*, 2010, **86**, 273–278.
19 J. J. Vallejo, M. Mesa and C. Gallardo, Evaluation of the avobenzone photostability in solvents used in cosmetic formulations, *Vitae*, 2011, **18**, 63–71.
20 J. Kockler, M. Oelgemöller, S. Robertson and B. D. Glass, Photostability of sunscreens, *J. Photochem. Photobiol., C*, 2012, **13**, 91–110.
21 N. A. Shaath, The chemistry of ultraviolet filters, in *Principles and Practice of Photoprotection*, ed. S. Q. Wang and H. W. Lim, Springer, Cham, Switzerland, 2016, pp. 143–157.
22 C. A. Bonda and D. Lott, Sunscreen photostability, in *Principles and Practice of Photoprotection*, ed. S. Q. Wang and H. W. Lim, Springer, Cham, Switzerland, 2016, pp. 247–273.
23 B. Herzog, D. Hueglin and U. Osterwalder, New sunscreen actives, in *Sunscreens, Regulations and Commercial Development*, ed. N. A. Shaath, Taylor & Francis, Boca Raton, 2005, pp. 291–320.
24 C. Tuchinda, H. W. Lim, U. Osterwalder and A. Rougier, Novel Emerging Sunscreen Technologies, *Derlmatol. Clin.*, 2006, **24**, 105–117.
25 G. Vielhaber, S. Grether-Beck, O. Koch, W. Johncock and J. Krutmann, Sunscreens with an absorption maximum of ≥360 nm provide optimal protection against UVA1-induced expression of matrix metalloproteinase-1, interleukin-1, and interleukin-6 in human dermal fibroblasts, *Photochem. Photobiol. Sci.*, 2006, **5**, 275–282.
26 A. Gallardo, J. Teixidó, R. Miralles, M. Raga, A. Guglietta, F. Marquillas, J. Sallarès and S. Nonell, Dose-dependent progressive sunscreens. A new strategy for photoprotection?, *Photochem. Photobiol. Sci.*, 2010, **9**, 530–534.
27 R. Jansen, U. Osterwalder, S. Q. Wang, M. Burnett and H. W. Lim, Photoprotection: Part II. Sunscreen: Development, efficacy, and controversies, *J. Am. Acad. Dermatol.*, 2013, **69**, 867.e1–867.e14.
28 B. P. Binks, P. D. I. Fletcher, A. J. Johnson, I. Marinopoulos, J. Crowther and M. A. Thompson, How the sun protection factor (SPF) of sunscreen films change during solar irradiation, *J. Photochem. Photobiol., A*, 2017, **333**, 186–199.
29 N. A. Shaath, Ultraviolet filters, *Photochem. Photobiol. Sci.*, 2010, **9**, 464–469.
30 U. Osterwalder, M. Sohn and B. Herzog, Global state of sunscreens, *Photodermatol., Photoimmunol. Photomed.*, 2014, **30**, 62–80.
31 S. Daly, H. Ouyang and P. Maitra, Chemistry of Sunscreens, in *Principles and Practice of Photoprotection*, ed. S. Q. Wang and H. W. Lim, Springer, Cham, Switzerland, 2016, pp. 159–178.
32 V. Lhiaubet-Vallet, M. Marin, O. Jimenez, O. Gorchs, C. Trullas and M. A. Miranda, Filter-filter interactions. Photostabilization, triplet quenching and reactivity with singlet oxygen, *Photochem. Photobiol. Sci.*, 2010, **9**, 552–558.
33 C. M. Kawakami, L. N. C. Máximo, B. B. Fontanezi, R. Santana da Silva and L. R. Gaspar, Diethylamino hydroxybenzoyl hexyl benzoate (DHHB) as additive to the UV filter avobenzone in cosmetic sunscreen formulations – Evaluation of the photochemical behavior and photostabilizing effect, *Eur. J. Pharm. Sci.*, 2017, **99**, 299–309.
34 A. Kikuchi, K. Shibata, R. Kumasaka and M. Yagi, Optical and time-resolved electron paramagnetic resonance studies of the excited states of a UV-B absorber (4-methylbenzylidene) camphor, *J. Phys. Chem. A*, 2013, **117**, 1413–1419.
35 A. Kikuchi, K. Shibata, R. Kumasaka and M. Yagi, Excited states of menthyl anthranilate: a UV-A absorber, *Photochem. Photobiol. Sci.*, 2013, **12**, 246–253.
36 T. Tsuchiya, A. Kikuchi, N. Oguchi-Fujiyama, K. Miyazawa and M. Yagi, Photoexcited triplet states of UV-B absorbers: ethylhexyl triazone and diethylhexylbutamido triazone, *Photochem. Photobiol. Sci.*, 2015, **14**, 807–814.
37 K. Sugiyama, T. Tsuchiya, A. Kikuchi and M. Yagi, Optical and electron paramagnetic resonance studies of the excited triplet states of UV-B absorbers: 2-ethylhexyl salicylate and homo menthyl salicylate, *Photochem. Photobiol. Sci.*, 2015, **14**, 1651–1659.
38 S. Pattanaargson, T. Munhapol, P. Hirunsupachot and P. Luangthongaram, Photoisomerization of octyl methoxycinnamate, *J. Photochem. Photobiol., A*, 2004, **161**, 269–274.
39 S.-Y. Hou, W. M. Hetherington III, G. M. Korenowski and K. B. Eisenthal, Intramolecular proton transfer and energy relaxation in ortho-hydroxybenzophenone, *Chem. Phys. Lett.*, 1979, **68**, 282–284.
40 M. Wiechmann, H. Port, W. Frey, F. Lärmer and T. Elsässer, Time-resolved spectroscopy on ultrafast proton transfer in 2-(2′-hydroxy-5′-methylphenyl)benzotriazole in liquid and polymer environments, *J. Phys. Chem.*, 1991, **95**, 1918–1923.

41 S. J. Formosinho and L. G. Arnaut, Excited-state proton transfer reactions II. Intramolecular reactions, *J. Photochem. Photobiol., A*, 1993, **75**, 21–48.
42 C. Chudoba, E. Riedle, M. Pfeiffer and T. Elsaesser, Vibrational coherence in ultrafast excited state proton transfer, *Chem. Phys. Lett.*, 1996, **263**, 622–628.
43 T. Okazaki, N. Hirota and M. Terazima, Picosecond time-resolved transient grating method for heat detection: Excited-state dynamics of $FeCl_3$ and *o*-hydroxybenzophenone in aqueous solution, *J. Phys. Chem. A*, 1997, **101**, 650–655.
44 A. A. Lamola and L. J. Sharp, Environmental effects on the excited states of o-hydroxy aromatic carbonyl compounds, *J. Phys. Chem.*, 1966, **70**, 2634–2638.
45 T. N. V. Karsili, B. Marchetti, M. N. R. Ashfold and W. Domcke, Ab initio study of potential ultrafast internal conversion routes in oxybenzone, caffeic acid, and ferulic acid: implications for sunscreens, *J. Phys. Chem. A*, 2014, **118**, 11999–12010.
46 P. Kottis and R. Lefebvre, Calculation of the electron spin resonance line shape of randomly oriented molecules in a triplet state. I. The $\Delta m = 2$ transition with a constant linewidth, *J. Chem. Phys.*, 1963, **39**, 393–403.
47 N. J. Turro, V. Ramamurthy and J. C. Scaiano, *Modern Molecular Photochemistry of Organic Molecules*, University Science Books, Sausalito, 2010.
48 D. G. Fresnadillo and S. Lacombe, Reference photosensitizers for the production of singlet oxygen, in *Singlet Oxygen: Applications in Biosciences and Nanosciences*, ed. S. Nonell and C. Flors, The Royal Society of Chemistry, Cambridge, UK, 2016, vol. 1, pp. 105–143.
49 S. Nonell and C. Flors, Steady-State and Time-Resolved Singlet Oxygen Phosphorescence Detection in the Near-IR, in *Singlet Oxygen: Applications in Biosciences and Nanosciences*, ed. S. Nonell and C. Flors, The Royal Society of Chemistry, Cambridge, UK, 2016, vol. 2, pp. 7–26.
50 M. Montalti, A. Credi, L. Prodi and M. T. Gandolfi, *Handbook of Photochemistry*, Tayler & Francis, Boca Raton, 2006.
51 R. Schmidt, Deactivation of $O_2(^1\Delta_g)$ singlet oxygen by carotenoids: Internal conversion of excited encounter complexes, *J. Phys. Chem. A*, 2004, **108**, 5509–5513.